Numerical and analytical estimates for the structure functions in two-dimensional magnetohydrodynamic flows

Rainer Grauer and Christiane Marliani
Institut für Theoretische Physik I, Heinrich-Heine-Universität Düsseldorf, D–40225 Düsseldorf, Germany

(Received 10 June 1994; accepted 16 August 1994)

In two-dimensional magnetohydrodynamic turbulence, the Kraichnan–Iroshnikov dimensional analysis suggests a linear scaling law for the exponents $\zeta_p = p/4$ of the structure functions for the Elsässer variables $\mathbf{z}^{\pm} = \mathbf{u} \pm \mathbf{B}$. Numerical simulations are presented and higher order structure functions are calculated using the extended self-similarity hypothesis of Benzi *et al.* [Phys. Rev. E **48**, R29 (1993)]. In addition, an estimate for the first structure function $\zeta_1 \geqslant 1/4$ is derived using a geometric technique introduced by Constantin and Procaccia [Phys. Rev. E **47**, 3307 (1993)] in the the context of the transport of a passive scalar in three-dimensional Navier–Stokes turbulence. © *1995 American Institute of Physics.*

I. INTRODUCTION AND MOTIVATION

Two-dimensional magnetohydrodynamic (MHD) flows play a distinguished role in the understanding of strong turbulence properties in high Reynolds number fluids. Unlike two-dimensional hydrodynamic flows, a mechanism for spontaneous amplification of vorticity and current density is present which may allow deviations from the phenomenological scaling introduced by Kraichnan[1] and Iroshnikov.[2] The two-dimensionality of the problem makes it numerically feasible and analytically simpler compared to the full three-dimensional problem.

The incompressible magnetohydrodynamic equations can be written in the form

$$\partial_t \mathbf{z}^{\pm} + \mathbf{z}^{\mp} \cdot \nabla \mathbf{z}^{\pm} + \nabla p = \nu \Delta \mathbf{z}^{\pm} \ , \quad \text{div } \mathbf{z}^{\pm} = 0, \tag{1}$$

where $\mathbf{z}^{\pm}$ denote the Elsässer variables $\mathbf{z}^{\pm} = \mathbf{u} \pm \mathbf{B}$. Here we assume a magnetic Prandtl number equal to one which places no restrictions on our analysis if we consider the inertial range.

One of the main differences between hydrodynamic and hydromagnetic turbulence is the interaction time τ. In hydromagnetic turbulence the interaction time τ is governed by the large scale magnetic field $\mathbf{B}_0$: $\tau \propto (B_0 k)^{-1}$. Small-scale fluctuations behave like Alfvén waves traveling in opposite directions. Assuming that the energy dissipation is proportional to the interaction time τ, dimensional analysis leads to the Kraichnan–Iroshnikov scaling for the structure functions of the Elsässer variables

$$\langle |\mathbf{z}^{\pm}(\mathbf{x}+\mathbf{l}) - \mathbf{z}^{\pm}(\mathbf{x})|^p \rangle \propto l^{\zeta_p} \ , \quad \zeta_p = \frac{p}{4} \ . \tag{2}$$

By analyzing satellite observations of MHD turbulence in the solar wind, Burlaga[3,4] and Marsch and Liu[5] demonstrated that the exponents ζ_p are nonlinear functions of p in contrast to the Kraichnan–Iroshnikov theory. A phenomenological multifractal cascade model has also been introduced by Carbone.[6]

Large-scale numerical investigations of two-dimensional magnetohydrodynamic flows have been undertaken by Biskamp and Welter[7] and Politano *et al.*[8] They address mainly the question whether or not the turbulent solutions display an energy spectrum consistent with the Kraichnan–Iroshnikov theory. Recently, high resolution simulations by Biskamp[9] have been analyzed with respect to the geometric properties of isocurrent density surfaces.

In this paper we present numerical simulations using a projection method based on a second-order upwind technique. This method is especially well suited for handling steep gradients which naturally arise in the formation of current sheets. We used the extended self-similarity hypothesis (ESS) of Benzi *et al.*[10] in order to calculate more accurately the exponents ζ_p. The results of our simulations support the presence of intermittency effects, i.e. we observed a nonlinear behavior of ζ_p on p.

Finally, we present a derivation of an estimate for the exponent of the first structure function ζ_1 based on a technique introduced by Constantin and Procaccia.[11,12] Work on higher structure functions is in progress.

II. NUMERICAL METHOD AND EXPERIMENTS

The two-dimensional magnetohydrodynamic equations (1) are solved in a rectangular box of size $L_x = L_y = 2\pi$ with periodic boundary conditions. Many numerical schemes for the calculation of turbulent fluid flow are based on a pseudospectral method using a leapfrog-Crank–Nicholson time stepping. These methods work correctly as long as no steep gradients develop in the flow. In that case they tend to produce oscillations which result in numerical instability. Therefore, the dissipation range must be well resolved, otherwise energy piles up at the bottom of the inertial range. In order to enlarge the inertial range we used a method which is stable even for discontinuous data. The scheme is based on a projection method proposed for the Navier–Stokes equations by Bell *et al.*[13] where the time stepping is performed in a second-order upwind manner. This method belongs to the class of shock capturing schemes and has successfully been applied to shear and variable density flows.[14] To demonstrate the ability of the method in handling steep gradients the upwind-time stepping is applied to the Burgers equation and compared to the results of a leapfrog integration. Figure 1 shows solutions propagating to the right of the two different simulations for smooth initial data. The spatial resolution

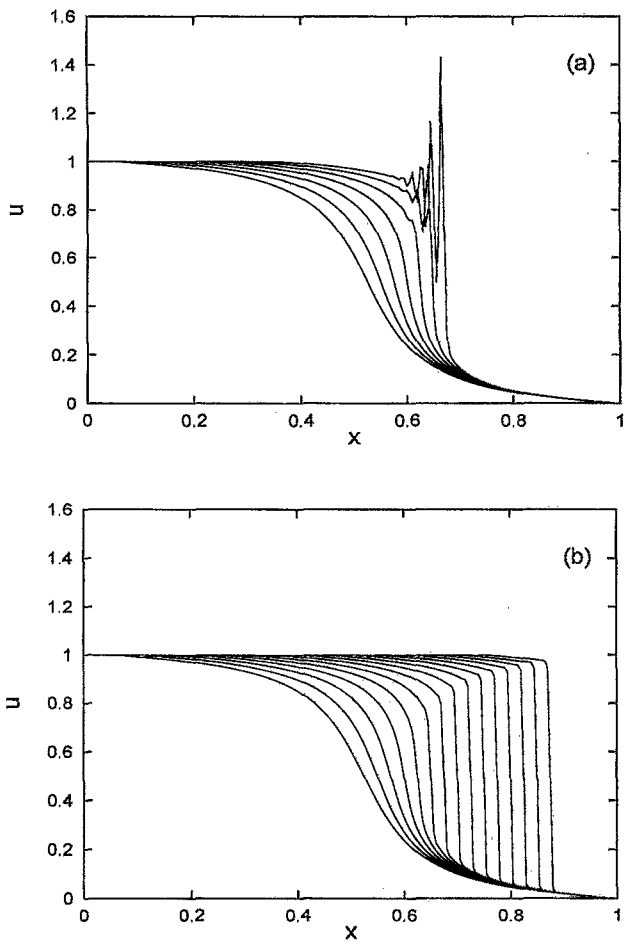

FIG. 1. Burgers equation integrated with the (a) leapfrog method and with the (b) second-order upwind-scheme.

Δx in the simulations is chosen as $\Delta x = 1/200$. In Fig. 1(a) solutions based on the leapfrog method develop oscillations when steep gradients start to form. On the other hand, the upwind-scheme is able to cope with the development of a shock front correctly. Of course, the upwind calculation introduces numerical dissipation which can be viewed as an additional subgrid viscosity. In the Burgers equation, the numerical viscosity ν_{num} based on the slope of the shock front is approximately given by $\nu_{\text{num}} = \Delta x/2$. But this quantity is of limited value since the shock front propagates with the correct velocity which suggests that no viscosity is present. For the MHD equations (1) the method works even in the absence of molecular viscosity and resistivity where dissipation is solely introduced by the numerical scheme.

In decaying turbulence the choice of the initial condition is of special relevance. An important criterion is the velocity-magnetic field correlation $\rho = |H|/E$ where $H = \int \mathbf{v}\cdot\mathbf{B}\, d^2x$ and E denotes the total energy. As Pouquet *et al.*[15] have shown, the energy spectra for the Elsässer variables exhibit different spectral indices in the inertial range if the correlation ρ is high. As a consequence E_k has no power law behavior. Biskamp and Welter[7] introduced initial conditions that show a stronger tendency to generate turbulent small-scale structures than the Orszag–Tang vortex. They have lower correlation and are made less symmetric by means of arbitrary phases. Therefore we choose

$$\phi^0(x,y) = \cos(x+1.4) + \cos(y+0.5),$$

$$\psi^0(x,y) = \tfrac{1}{3}[\cos(2x+2.3) + \cos(y+4.7)],$$

as initial conditions for the magnetic flux function ψ, $\mathbf{B} = \mathbf{e}_z \times \nabla\psi$, and the velocity streamfunction ϕ, $\mathbf{v} = \mathbf{e}_z \times \nabla\phi$ denoted as A_2 in Biskamp and Welter.[7] Initially, the value of the correlation coefficient is given by $\rho = 0.13$. It grows to a value of $\rho = 0.16$ at the end of the run.

Our numerical studies of decaying two-dimensional magnetohydrodynamic turbulence were performed with up to 512×512 grid points for two different values of the kinematic viscosity: $\nu = 6.25 \times 10^{-4}$ and $\nu = 0$. The magnetic Prandtl number was chosen to 1 in each case. In the time interval where all statistical evaluations were performed the resulting magnetic and kinetic microscale Reynolds numbers are $R_\lambda^m = 382$ and $R_\lambda^k = 175$ for $\nu = 6.25 \times 10^{-4}$ and $R_\lambda^m = 656$ and $R_\lambda^k = 300$ for $\nu = 0$.

Contour plots of the typical time evolution of the current density are shown in Fig. 2. First, current sheets develop until reconnection takes place by a tearing instability which results in the production of small-scale turbulence. The large-scale structure of the flow is similar in both runs, e.g. $\nu = 6.25 \times 10^{-4}$ and $\nu = 0$, whereas the small-scale fluctuations and intermittency effects are much better resolved in the $\nu = 0$ run. The amount of numerical dissipation can be estimated by the formula

$$\nu = -\frac{\partial_t E}{W},$$

where $W = \int (|\nabla \times \mathbf{u}|^2 + |\nabla \times \mathbf{B}|^2) dx dy$ denotes the total enstrophy of the flow. For the $\nu = 0$ run, we obtain a numerical viscosity $\nu_{\text{num}} = 2 \times 10^{-4}$. To achieve this viscosity with a leapfrog-Crank–Nicholson scheme, a spatial resolution of 1024^2 grid points would be needed. All statistical averages have been performed when the small-scale turbulence was well developed. For the initial conditions chosen here, temporal averages were taken between $t = 6.0$ and $t = 8.0$. In this time interval, the enstrophy is approximately constant as can be seen in Fig. 3. Also, the energy spectra depicted in Fig. 4 show only slight variations in time and indicate that the flow is well resolved. Figures 5 and 6 show the temporal evolution of the total energy and the correlation coefficient, respectively.

Our main objective is to study the behavior of the structure functions of order p defined as $\langle |z^{\pm}(\mathbf{x}+\mathbf{l}) - z^{\pm}(\mathbf{x})|^p \rangle$, where $z^{\pm}(\mathbf{x})$ is the component parallel to the displacement $\mathbf{l}$ and $\langle \ldots \rangle$ denotes spatial and temporal averaging. In the inertial subrange one expects a power law behavior

$$\langle |z^{\pm}(\mathbf{x}+\mathbf{l}) - z^{\pm}(\mathbf{x})|^p \rangle \propto l^{\zeta_p} \tag{3}$$

with $l = |\mathbf{l}|$ and scaling exponent ζ_p.

As extended inertial ranges are only observed at very large Reynolds numbers, the direct calculation of the exponents ζ_p is very difficult. Our numerical data only allows for a crude estimate of the exponents, because choosing the fit-

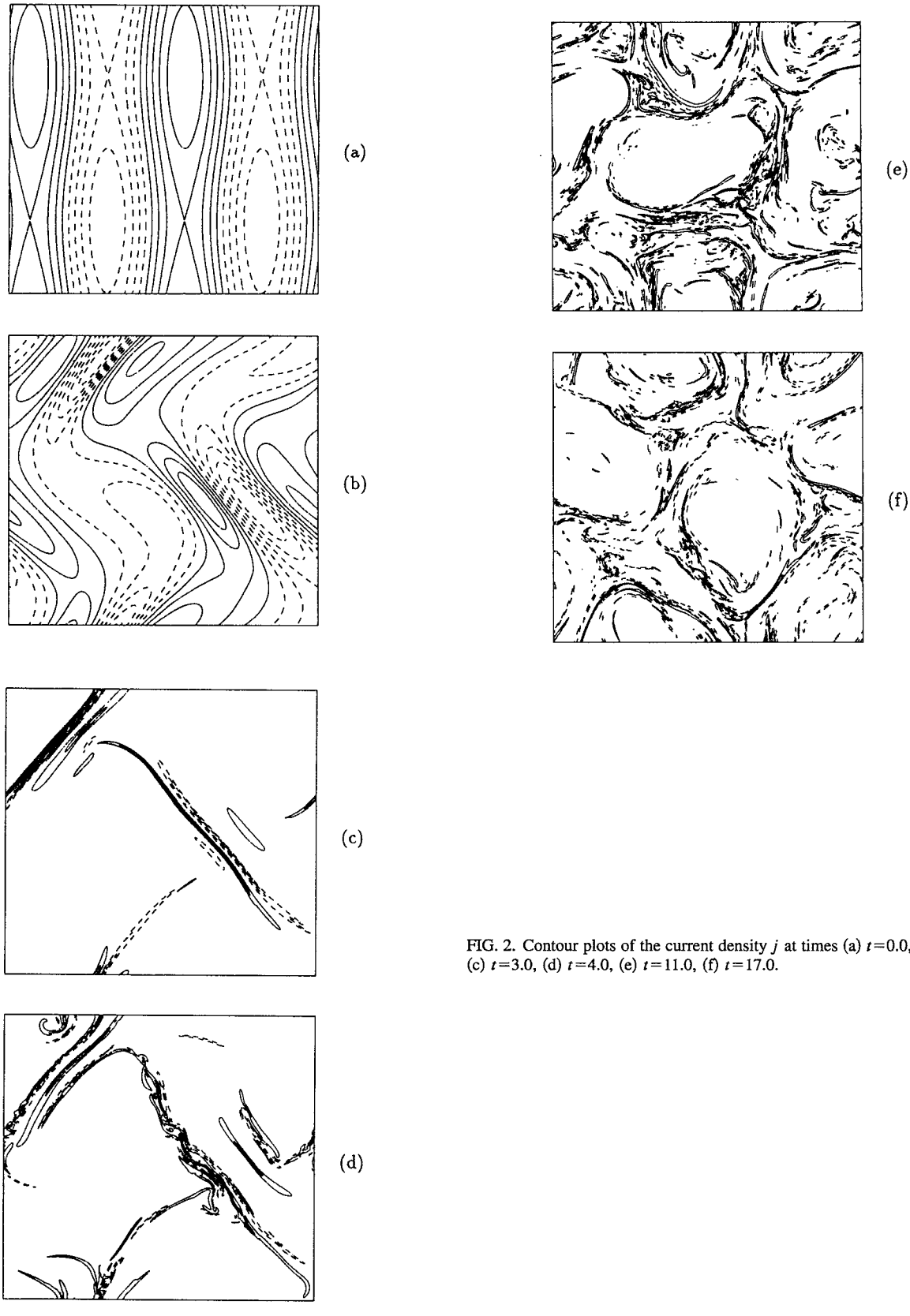

FIG. 2. Contour plots of the current density j at times (a) $t=0.0$, (b) $t=1.0$, (c) $t=3.0$, (d) $t=4.0$, (e) $t=11.0$, (f) $t=17.0$.

ting range involves a considerable uncertainty. We show an example of the second structure function plotted against l and a fit with a straight line $l^{1/2}$ in a log–log plot in Fig. 7. This figure indicates the need for higher spatial resolution (which would enlarge the inertial range) as well as the need for longer time intervals to perform temporal averages.

To circumvent this difficulty we make use of an extended self-similarity hypothesis (ESS) introduced for the

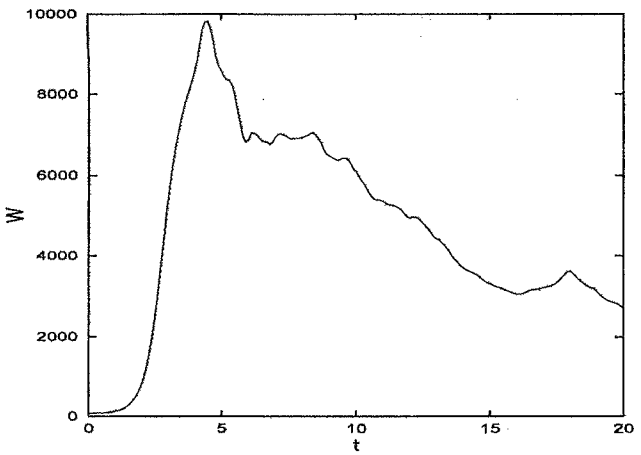

FIG. 3. Time evolution of enstrophy for the zero viscosity run.

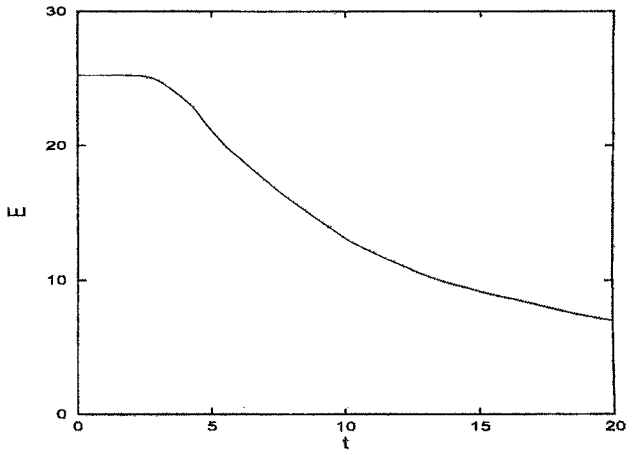

FIG. 5. Time evolution of energy for the zero viscosity run.

case of hydrodynamic turbulence by Benzi *et al.*[16] The interesting quantity is the relation between the structure functions of different order which can be written in the form

$$\langle|z^{\pm}(\mathbf{x}+\mathbf{l})-z^{\pm}(\mathbf{x})|^{n}\rangle=\langle|z^{\pm}(\mathbf{x}+\mathbf{l})-z^{\pm}(\mathbf{x})|^{m}\rangle^{\beta_{nm}} \qquad (4)$$

where $\beta_{nm}=\zeta_n/\zeta_m$. In the inertial range, Eq. (4) is a direct consequence of the power law behavior (3). The hypothesis of extended self-similarity now consists of assuming that relation (4) holds also in the viscous subrange. Our numerical simulations indicate that the self-similarity hypothesis applies to MHD turbulence as well. This can clearly be seen in Fig. 8 where the third- and fourth-order structure functions are plotted against the second-order structure function in a double logarithmic graph. The assumption of the extended self-similarity hypothesis allows a much more precise computation of the exponents ζ_p once a single scaling exponent is known. In hydrodynamic turbulence, the analytically known value for the third-order scaling exponent $\zeta_3=1$ can be used as a reference for evaluating β_{nm} by means of ESS. The application of Kolmogorov's refined similarity hypothesis[17] to magnetohydrodynamic turbulence suggests the relation $\zeta_4=1$ (see e.g. Carbone[18]) which will be used as a reference in calculating the other scaling exponents.

Figure 9 shows the scaling exponents as a function of p for the Elsässer variable $z^{\pm}$ in the y-direction obtained with the assumption of extended self-similarity. Although the exponents contain the uncertainty mentioned above, a deviation from a linear law of the Kraichnan–Iroshnikov theory is clearly visible, indicating the intermittency in the flow.

III. GEOMETRIC THEORY

In this section we apply a method introduced by Constantin and Procaccia[11,12] to estimate the exponent ζ_1 of the first structure function for the Elsässer variables $\mathbf{z}^{\pm}$. In Ref. 11 this method was used in the calculation of a passive scalar transported by the velocity field of the three-dimensional Navier–Stokes equations. Here, we apply the method directly to the active fields $\mathbf{z}^{\pm}$ where — in contrast to the transport of a passive scalar — the pressure field has to be estimated as well. We use a similar notation as in Ref. 11 to keep the calculation as transparent as possible. In order to

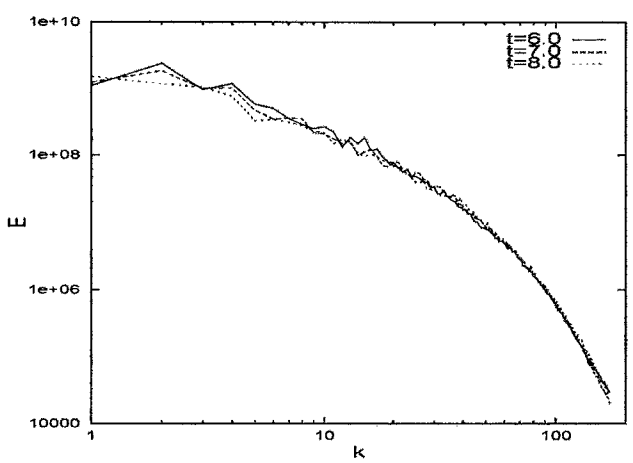

FIG. 4. Energy spectra at times $t=6.0$, $t=7.0$ and $t=8.0$.

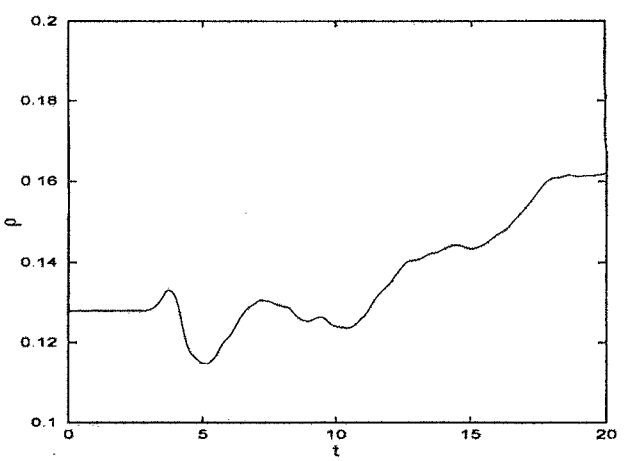

FIG. 6. Time evolution of the correlation coefficient.

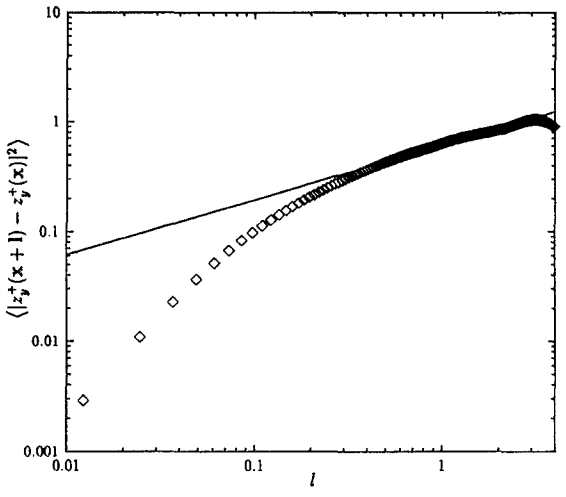

FIG. 7. Second-order structure function versus l for the y-component of $\mathbf{z}^+$ at kinetic Reynolds number $R_\lambda^k=656$ and best fit $l^{0.5}$.

describe a statistical stationary state, a forcing term has to be added to the MHD Eqs. (1). Again, we restrict ourselves to the case of magnetic Prandtl number 1 so that the MHD equations under consideration take the form

$$\partial_t \mathbf{z}^{\pm}+\mathbf{z}^{\mp}\cdot\nabla\mathbf{z}^{\pm}+\nabla p=\nu\Delta\mathbf{z}^{\pm}+\mathbf{F}^{\pm}\ ,\quad \text{div}\ \mathbf{z}^{\pm}=0. \tag{5}$$

The first calculation relates the time-averaged Hausdorff-dimension $\bar{D}_G$ of the graph $G^{\pm}$ of the Elsässer variables

$$G^{\pm}(B)=\{(\mathbf{x},\mathbf{z}^{\pm}(\mathbf{x}))|\mathbf{x}\in B\}$$

to the exponent of the first structure function ζ_1. For the two-dimensional MHD Eqs. (5) where

$$\mathbf{z}^{\pm}:\mathbf{R}^2\subset\Omega\rightarrow\mathbf{R}^2,$$

direct application of the calculation in[11,19] gives the inequality

$$\bar{D}_G\leqslant 2+2(1-\zeta_1)=4-2\zeta_1\,. \tag{6}$$

The two-dimensional Hausdorff measure of $G^{\pm}(B)$ can be calculated by use of the area formula

$$H^{(2)}(G^{\pm}(B))=\int_B J(\mathbf{x})d^2x\ , \tag{7}$$

where $J(\mathbf{x})$ is the root of the Jacobian

$$J^2(\mathbf{x})=\det\left[\delta_{ij}+\frac{\partial\mathbf{z}^{\pm}}{\partial x_i}\frac{\partial\mathbf{z}^{\pm}}{\partial x_j}\right]_{i,j=1,2}.$$

The Jacobian can be expressed by the invariants I_k of the matrix $[(\nabla\mathbf{z}^{\pm})^*(\nabla\mathbf{z}^{\pm})]$. In the two-dimensional case considered here, they can be written as

$$I_1=\text{tr}[(\nabla\mathbf{z}^{\pm})^*(\nabla\mathbf{z}^{\pm})],$$

$$I_2=\det[(\nabla\mathbf{z}^{\pm})^*(\nabla\mathbf{z}^{\pm})],$$

$$I_k=0\quad\text{for}\quad k\geqslant 3\ .$$

In terms of the invariants the Jacobian takes the simple form

$$J^2(\mathbf{x})=1+I_1+I_2\,.$$

For the time-dependent field $\mathbf{z}^{\pm}$ the graph $G^{\pm}(B)$ and the Hausdorff measure of the graph are also functions depending on time. Since we are interested in the exponent ζ_1 of the first structure function which results from temporal averaging we have to calculate the time-averaged Hausdorff measure

$$\langle H^{(2)}(G^{\pm}(B,t))\rangle=\left\langle\int_B J(\mathbf{x},t)d^2x\right\rangle. \tag{8}$$

To obtain an expression for the averaged Hausdorff measure of $G^{\pm}(B,t)$ we first multiply Eq. (5) with $\mathbf{z}^{\pm}$ from which it follows that

$$\tfrac{1}{2}\partial_t(\mathbf{z}^{\pm})^2+\mathbf{z}^{\pm}\cdot(\mathbf{z}^{\mp}\cdot\nabla\mathbf{z}^{\pm})=\nu\mathbf{z}^{\pm}\cdot\Delta\mathbf{z}^{\pm}-\mathbf{z}^{\pm}\cdot\nabla p+\mathbf{z}^{\pm}\cdot\mathbf{F}^{\pm}\ .$$

This can be transformed into

$$\tfrac{1}{2}(\partial_t+\mathbf{z}^{\mp}\cdot\nabla-\nu\Delta)(\mathbf{z}^{\pm})^2+\nu|\nabla\mathbf{z}^{\pm}|^2+\mathbf{z}^{\pm}\cdot\nabla p=\mathbf{z}^{\pm}\cdot\mathbf{F}^{\pm}\ . \tag{9}$$

Introducing a cutoff function

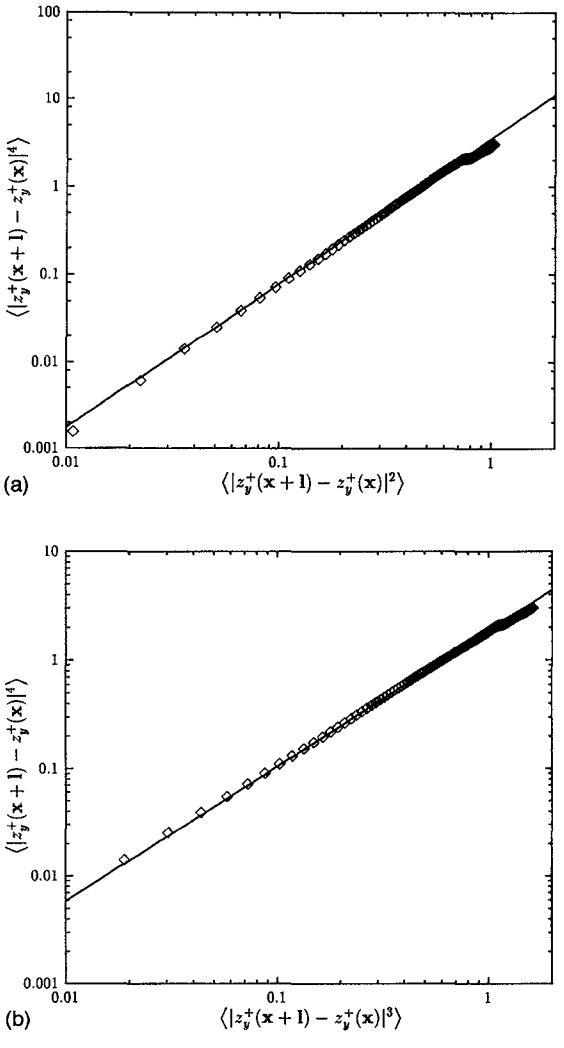

FIG. 8. Fourth-order against second-order (a) and third-order (b) structure function for the y-component of $\mathbf{z}^+$ at kinetic Reynolds number $R_\lambda^k=656$.

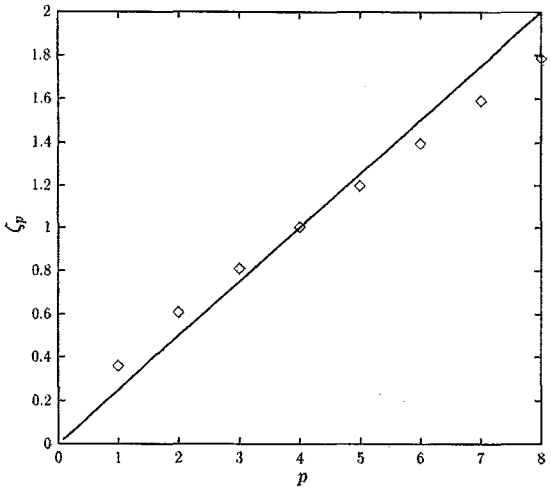

FIG. 9. Scaling exponent ζ_p for the y-component of $\mathbf{z}^+$ versus p. The linear function corresponds to the Kraichnan–Iroshnikov scaling $\zeta_p = p/4$.

$$\chi(\mathbf{y}) = \begin{cases} 1 & \text{for } |\mathbf{y}| \leqslant 1, \\ 0 & \text{for } |\mathbf{y}| \geqslant 2, \end{cases}$$

and integrating over space, one yields

$$\int |\nabla \mathbf{z}^{\pm}|^2(\mathbf{x}) \chi\left(\frac{\mathbf{x}-\mathbf{x}_0}{\rho}\right) d^2x$$

$$= -\frac{1}{2\nu} \int \chi\left(\frac{\mathbf{x}-\mathbf{x}_0}{\rho}\right) [(\partial_t + \mathbf{z}^{\mp} \cdot \nabla - \nu\Delta)(\mathbf{z}^{\pm})^2$$

$$+ 2\mathbf{z}^{\pm} \cdot \nabla p - 2\mathbf{z}^{\pm} \cdot \mathbf{F}^{\pm}] d^2x \, . \tag{10}$$

The five expressions on the right hand side of Eq. (10) have to be estimated separately. We introduce the variable $\mathbf{y} = (\mathbf{x}-\mathbf{x}_0)/\rho$ so that the expressions take the form

$$S_1(\mathbf{x}_0,\rho,t) = -\frac{1}{2\nu} \frac{d}{dt} \int \chi(\mathbf{y}) (\mathbf{z}^{\pm})^2 d^2x,$$

$$S_2(\mathbf{x}_0,\rho,t) = -\frac{1}{2\nu} \int \chi(\mathbf{y}) \mathbf{z}^{\mp} \cdot \nabla (\mathbf{z}^{\pm})^2 d^2x$$

$$= \frac{1}{2\nu\rho} \int (\mathbf{z}^{\pm})^2 z_j^{\mp} \left[\frac{\partial \chi}{\partial y_j}\right](\mathbf{y}) d^2x,$$

$$S_3(\mathbf{x}_0,\rho,t) = \frac{1}{2} \int \chi(\mathbf{y}) \Delta (\mathbf{z}^{\pm})^2 d^2x$$

$$= \frac{1}{2\rho^2} \int (\mathbf{z}^{\pm})^2 (\Delta_y \chi)(\mathbf{y}) d^2x,$$

$$S_4(\mathbf{x}_0,\rho,t) = \frac{1}{\nu} \int \chi(\mathbf{y}) \mathbf{z}^{\pm} \cdot \mathbf{F}^{\pm} d^2x,$$

$$S_5(\mathbf{x}_0,\rho,t) = -\frac{1}{\nu} \int \chi(\mathbf{y}) \mathbf{z}^{\pm} \cdot \nabla p d^2x.$$

Defining

$$\mathcal{Z} = \sup_{\mathbf{x},t} [\max(|\mathbf{z}^+|, |\mathbf{z}^-|)]$$

and

$$\mathcal{F} = \sup_{\mathbf{x},t} [\max(|\mathbf{F}^+|, |\mathbf{F}^-|)]$$

leads immediately to

$$|S_2(\mathbf{x},\rho,t)| \leqslant C_1 \frac{\mathcal{Z}^3 \rho}{\nu},$$

$$|S_3(\mathbf{x},\rho,t)| \leqslant C_2 \mathcal{Z}^2,$$

$$|S_4(\mathbf{x},\rho,t)| \leqslant C_3 \frac{\mathcal{Z}\mathcal{F}\rho^2}{\nu}.$$

The constants C_1, C_2, C_3 depend only on $\int |\nabla_y \chi| d^2y$, $\int |\Delta_y \chi| d^2y$ and $\int |\chi| d^2y$. By averaging in time the first term $S_1(\mathbf{x},\rho,t)$ vanishes and we get

$$\langle S_1 \rangle = 0, \tag{11}$$

$$\langle |S_2| \rangle \leqslant C_1 \frac{\mathcal{Z}^3 \rho}{\nu}, \tag{12}$$

$$\langle |S_3| \rangle \leqslant C_2 \mathcal{Z}^2, \tag{13}$$

$$\langle |S_4| \rangle \leqslant C_3 \frac{\mathcal{Z}\mathcal{F}\rho^2}{\nu}. \tag{14}$$

Finally, we have to estimate the pressure term $S_5(\mathbf{x}_0,\rho,t) = -(1/\nu) \int \chi(\mathbf{y}) \mathbf{z}^{\pm} \cdot \nabla p d^2x$. To achieve this we decompose $\chi \mathbf{z}^{\pm}$ into a divergence free and curl free part

$$\chi(\mathbf{y}) \mathbf{z}^{\pm} = \mathbf{e}_z \times \nabla f_1 + \nabla f_2 \tag{15}$$

and take the divergence

$$\nabla \cdot (\chi(\mathbf{y}) \mathbf{z}^{\pm}) = \Delta f_2 = \mathbf{z}^{\pm} \cdot \nabla \chi(\mathbf{y}). \tag{16}$$

Assuming the forces $\mathbf{F}^{\pm}$ as divergence free the pressure solves the elliptic equation $-\Delta p = \nabla \cdot (\mathbf{z}^{\mp} \cdot \nabla \mathbf{z}^{\pm})$ so that the pressure integral takes the form

$$\int \chi(\mathbf{y}) \mathbf{z}^{\pm} \cdot \nabla p d^2x$$

$$= -\int \Delta f_2 p d^2x = -\int f_2 \Delta p d^2x$$

$$= \int f_2 \nabla \cdot (\mathbf{z}^{\mp} \cdot \nabla \mathbf{z}^{\pm}) d^2x = \int (\partial_i \partial_j f_2) z_j^{\mp} z_i^{\pm} d^2x$$

$$\leqslant C_4' \mathcal{Z}^2 \rho^{1/2} \left(\sum_{i,j} \int |\partial_i \partial_j f_2|^2 d^2x \right)^{1/2}$$

$$\leqslant C_4'' \mathcal{Z}^2 \rho^{1/2} \left(\int |\Delta f_2|^2 d^2x \right)^{1/2} \leqslant C_4 \mathcal{Z}^3 \rho \, , \tag{17}$$

where the constant C_4 depends only on $(\int |\nabla_y \chi|^2 d^2y)^{1/2}$. We denote the length scale on which the largest variations of $\mathbf{z}^{\pm}$ occur by L.

Inserting the results (11)–(14), and (17) and choosing $\rho = L$ gives the estimate

$$\left\langle \int_{B_L} |\nabla \mathbf{z}^{\pm}|^2(\mathbf{x}) d^2x \right\rangle \leqslant C \mathcal{Z}^2 \left(\frac{L\mathcal{Z}}{\nu} + 1 \right) + C' \frac{L^2 \mathcal{Z}\mathcal{F}}{\nu}. \tag{18}$$

The last term of Eq. (18) can be neglected if $\mathscr{Z}^2 \gg L\mathscr{F}$. This corresponds to the situation that the graph is the most wrinkled far from the production range. Defining the Reynolds number R_Λ as $L\mathscr{Z}/\nu$ and assuming $R_\Lambda \gg 1$ gives the relation

$$\left\langle \int_{B_L} |\nabla \mathbf{z}^{\pm}|^2(\mathbf{x}) d^2x \right\rangle \leqslant C\mathscr{Z}^2 R_\Lambda . \tag{19}$$

The number of degrees of freedom is given by $N=(L/r_0)^2$, where r_0 denotes the dissipation length. It can be shown by counting the number of unstable modes that the number of degrees of freedom obeys $N \geqslant CR_\Lambda^{4/3}$ from which follows $R_\Lambda \leqslant C(L/r_0)^{3/2}$ so that Eq. (19) takes the form

$$\left\langle \int_{B_L} |\nabla \mathbf{z}^{\pm}|^2(\mathbf{x}) d^2x \right\rangle \leqslant C\mathscr{Z}^2 \left(\frac{L}{r_0}\right)^{3/2} . \tag{20}$$

The final step involves the calculation of the two-dimensional Hausdorff measure $H^{(2)}(G(B))$

$$H^{(2)}(G(B)) = \int_B J(\mathbf{x}) d^2x$$

with

$$J^2(\mathbf{x}) = 1 + I_1(\mathbf{x}) + I_2(\mathbf{x}).$$

Inserting the definitions of the invariants and averaging in time yields the estimate

$$\langle H^{(2)}(G(B))\rangle \leqslant 1 + \left\langle \int_B (\mathrm{tr}[(\nabla \mathbf{z}^{\pm})^* \cdot (\nabla \mathbf{z}^{\pm})])^{1/2} d^2x \right\rangle + \left\langle \int_B (\det[(\nabla \mathbf{z}^{\pm})^* \cdot (\nabla \mathbf{z}^{\pm})])^{1/2} d^2x \right\rangle .$$

The second term on the right hand side can be absorbed into the third one which can be estimated in the two-dimensional divergence free case as

$$\left\langle \int_{B_L} (\det[(\nabla \mathbf{z}^{\pm})^* \cdot (\nabla \mathbf{z}^{\pm})])^{1/2} d^2x \right\rangle \leqslant \left\langle \int_{B_L} |\nabla \mathbf{z}^{\pm}|^2 d^2x \right\rangle .$$

By the definition of the Hausdorff dimension the additional inequality holds

$$\langle H^{(2)}(G(B))\rangle \geqslant \mathscr{Z}^2 \left(\frac{L}{r_0}\right)^{\bar{D}_G - 2} .$$

Combining the inequalities gives an estimate for the Hausdorff dimension $\bar{D}_G$

$$\bar{D}_G - 2 \leqslant \tfrac{3}{2}.$$

Assuming the inequality (6) to be sharp gives the final estimate for the exponent of the first structure function

$$\zeta_1 \geqslant \tfrac{1}{4} . \tag{21}$$

ACKNOWLEDGMENTS

This work was performed under the auspices of the Sonderforschungsbereich 191. The work of R. Grauer was supported by the Minister of Science of Nordrhein–Westfalen through the Bennigsen–Foerder Preis.

[1] R. H. Kraichnan, Phys. Fluids **8**, 1385 (1965).
[2] P. S. Iroshnikov, Sov. Astron. **7**, 566 (1964).
[3] L. F. Burlaga, J. Geophys. Res. **96**, 5847 (1991).
[4] L. F. Burlaga, J. Geophys. Res. **97**, 4283 (1992).
[5] E. Marsch and S. Liu, Ann. Geophys. **11**, 227 (1993).
[6] V. Carbone, Phys. Rev. Lett. **71**, 1546 (1993).
[7] D. Biskamp and H. Welter, Phys. Fluids B **1**, 1964 (1989).
[8] H. Politano, A. Pouquet, and P. L. Sulem, Phys. Fluids B **1**, 2330 (1989).
[9] D. Biskamp, Europhys. Lett. **21**, 563 (1993).
[10] R. Benzi, S. Ciliberto, C. Baudet, G. R. Chavarria, and R. Tripiccione, Europhys. Lett. **4**, 275 (1993).
[11] P. Constantin and I. Procaccia, Phys. Rev. E **47**, 3307 (1993).
[12] I. Procaccia and P. Constantin, Phys. Rev. Lett. **70**, 3416 (1993).
[13] J. B. Bell, P. Colella, and H. M. Glaz, J. Comput. Phys. **85**, 257 (1989).
[14] J. B. Bell and D. L. Marcus, J. Comput. Phys. **101**, 334 (1992).
[15] A. Pouquet, P. L. Sulem, and M. Meneguzzi, Phys. Fluids **31**, 2635 (1988).
[16] R. Benzi, S. Ciliberto, R. Tripiccione, C. Baudet, F. Massaioli, and S. Succi, Phys. Rev. E **48**, R29 (1993).
[17] A. N. Kolmogorov, J. Fluid Mech. **13**, 82 (1962).
[18] R. E. Caflisch, Physica D **67**, 1 (1993).
[19] K. J. Falconer, *The Geometry of Fractal Sets* (Cambridge University Press, Cambridge, 1985).